Stiffness and toughness gradation of bamboo from a damage tolerance perspective

Sayyad Mannan, Venkitanarayanan Parameswaran, Sumit Basu*

Department of Mechanical Engineering, Indian Institute of Technology Kanpur, Kanpur 208016, Uttar Pradesh, India.

Abstract

Typical bamboo plants, in order to gain phototropic advantage over other land plants, are known to achieve heights of up to 20 m. They have also evolved radially graded and have almost transversely isotropic elastic properties (with the longitudinal direction being the axis of isotropy) primarily owing to the areal distribution of fibre bundles. These bundles are densely packed in the outer periphery of the cross section and sparsely in the inner. As shown in a previous work (Mannan et al., 2016), the axial modulus of a bamboo culm can be estimated from a careful measurement of the angle that cellulose microfibrils make with the axis of the fibres and their areal density distribution. In the first part of this paper, using these micromechanical estimates as the starting point and a combination of digital image correlation and Finite Element simulations, more complete information about the overall stiffness of a culm and its variation across the radius is obtained. Further, these stiffness measurements are used to determine crack resistance curves for almost all crack growth and loading direction combinations possible in a radially graded, transversely isotropic material. Finally, these fracture toughness measurements are used to show how the radially graded stiffness and toughness helps bamboo to convert flaws of all orientations into ones that propagate in a splitting mode along the length of the fibres. It is surmised that, under bending loads, the fracture toughnesses in various orientations have evolved in a manner as to trigger easy kinking of all flaws to the longitudinal direction.

Keywords: Bamboo; Functionally graded material; Mechanical properties; Fracture properties; Structure-property-function correlations

1. Introduction

Bamboo is a tall and slender land plant with a hollow, circular and gently tapering stem. Like many other natural materials, bamboo too is a multiscale composite (see, Fig. 1). The basic building block at the lowest length scale is a composite material consisting of very strong and mostly single crystalline cellulose in a hemicellulose-lignin matrix. Using a toolbox consisting of this basic building block, like in many other natural materials (Wegst et al., 2014), a strong and tough structure is synthesised. At the macroscopic level, the major contributors to the stiffness are bundles of fibrils oriented almost parallel to the axial direction. These bundles are close packed groups of circular fibrils, which in turn, are basically dense sclerenchyma cells reinforced by favourably aligned cellulose-hemicellulose-lignin building blocks. These fibre bundles are interspersed in a matrix composed of prismatic, hollow and thin-walled parenchymatous cells. The matrix resembles closed-cell foam. The parenchyma cell

*Corresponding author

Email address: sbasu@iitk.ac.in (Sumit Basu)

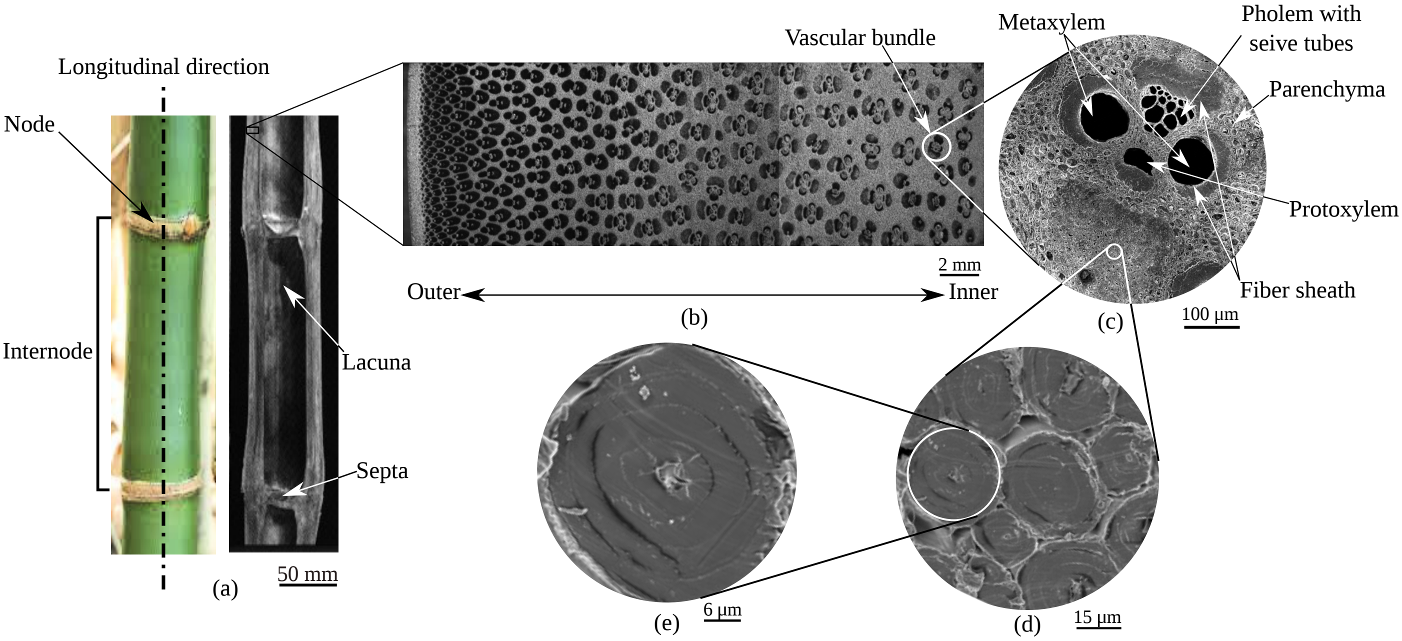

Figure 1: A longitudinal section bamboo is shown in (a). The cross-section (b) has graded distribution of fibre bundles, denser at the outer radial location. Fibre bundles actually form sheaths around vascular tubes (c). The bundles themselves consist of close packed, almost circular sclerenchyma cells called fibrils (d) which are lamellar structures (e) with different orientations of the basic cellulose-hemicellulose-lignin building blocks in each lamella.

walls are also reinforced by the basic building block, albeit oriented less favourably than in the fibrils. Moreover, the fibre bundles are not uniformly dispersed in the matrix but are denser towards the outer periphery. The overall structure allows us to characterise bamboo as a fibre-reinforced, functionally graded, transversely isotropic material (the plane of isotropy being perpendicular to the longitudinal direction) with gradation in properties in the radial direction (see also, Liese, 1998 for a comprehensive discussion of the complete anatomy of a bamboo culm).

In a recent work (Mannan et al., 2016) (see also related works by Silva et al., 2008; Tan et al., 2011), it has been shown that the variation of the graded longitudinal stiffness along the radius closely correlates with the variation in the volume fraction of the fibre bundles. Moreover, the magnitude of the longitudinal stiffness depends on the mean fibril angle (MFA), which is the average orientation of the basic building blocks (i.e. the cellulose-hemicellulose-lignin composite) about the longitudinal axis. In a separate work (Mannan et al., 2017), the MFA at fine resolution over the fibril as well as the parenchyma cell walls has been mapped for a particular species of bamboo. While MFA $\bar{\mu}$ is around 15° $(4-29^\circ)$ in the fibrils, it is much larger (about 35°) in the parenchyma walls. As will be seen later, the average longitudinal stiffness of this species of bamboo turns out to be of the order of 10.9 GPa. This is almost an order of magnitude superior to its averaged transverse stiffness.

The high stiffness of bamboo in the longitudinal direction is, for its survival, an important property. Bamboo can grow as tall as $10-20$ m and has to bear its self weight as well as significant bending loads due to external forces due to wind. Maximising its ability to bend while keeping the self weight low seems to be a smart evolutionary strategy that bamboo (and many other plants like palms, see Wegst, 2011) has adopted. It can be shown that (following Wegst, 2011) for the same mass per unit length, bamboo has about 5 times more stiffness in bending compared to a solid circular rod made of the cell wall material. This is mainly because of the fact that much of the matrix in bamboo is made up of cellular parenchyma, which reduces its overall density significantly.

The rationale behind the so-called 'stellar' arrangement of the fibre bundles in order to achieve radially graded stiffness is more subtle. Wegst (2011) makes a comparison between the bending stiffness of a beam with graded longitudinal stiffness with one that has homogeneous stiffness (with the value being the average of the graded stiffness) and shows, that for the typical dimensions of the bamboo cross-section, grading may afford a further 30% increase in flexural rigidity. Thus, a stellar arrangement of fibres and a cellular matrix together, adds up to a very significant advantage in terms of flexural rigidity.

As far as its mechanical efficiency as a natural material is concerned, bamboo is superior to most other natural materials in terms of the specific modulus i.e. the ratio of its Young's modulus and density. This suggests that as a tie in tension, bamboo is very well suited. But, if its efficiency as a beam in flexure is considered, balsa wood, coconut timber and other kinds of timber are superior. In terms of specific strength too (i.e. strength to density ratio), many varieties of silk are superior. However, based on the limited data available on the fracture of natural materials, bamboo turns out to be extremely efficient. Thus, in terms of both load and displacement at failure (Wegst and Ashby, 2004), bamboo ranks above most natural materials including woods, nut shells and cuticle. This observation motivates us to investigate the fracture properties of bamboo further and seek a possible connection between the gradation of properties in the radial direction and fracture.

Cracks in bamboo grow along interfaces between fibre bundles and parenchyma as well as parenchyma and parenchyma. Additionally, the fracture toughness of bamboo also seems to be radially graded. Amada and Untao (2001) have experimentally evaluated fracture toughness K_{Ic} of *Mouso* bamboo (*Phyllostachys edulis* Riv.) and observed that K_{Ic} forms a functionally graded structure. For *Moso* bamboo, both energy release rate (Tan et al., 2011) and crack opening displacement (Zhao et al., 2011) are larger in the low fibre density inner region. Also, the interlaminar fracture toughness in a similar species is known to be rather low in Mode-I (Shao et al., 2009) though under Mode-II the toughness increases significantly. In summary, the splitting modes of failure have lower toughness than the transverse (fibre-cutting modes) modes while all toughness values are graded in the radial direction.

Like in wood (Gibson and Ashby, 1997), several modes of crack propagation can be identified in bamboo. This is shown in Fig. 2. The axis of transverse isotropy is the longitudinal or L direction. The properties are graded in the radial or R direction. Fracture samples can be cut from the culm in the manner shown in the figure. Each sample is denoted by a pair of letters, the first of which is the direction normal to the crack plane and the second gives the direction of crack propagation. The gradation in colour indicates the gradation in fibre density; dark is more dense. In fibre-cutting modes like LR, a + or − sign indicates cases where the crack is on the rarer or denser side, respectively. A complete characterisation will require the determination of toughnesses for all the crack orientations and propagation directions shown. This task in this paper is accomplished for a specific variety of bamboo.

A larger question is how the survival of bamboo is affected by the toughnesses in the various modes and in particular, by the gradation in these properties in the radial direction. Through a combination of simple fracture mechanics based arguments and some Finite Element (FE) simulations, a plausible answer is provided to the question "Why is bamboo functionally graded?"

The paper is organised in the following manner. In a recent work (Mannan et al., 2016), the longitudinal stiffness of bamboo has been characterised, using information about the stiffness of the basic building block (i.e. the cellulose-hemicellulose-lignin complex), the MFA measurements in various cell walls and the areal distribution of fibre bundles over the cross-section. In Sec. 2, the use of digital

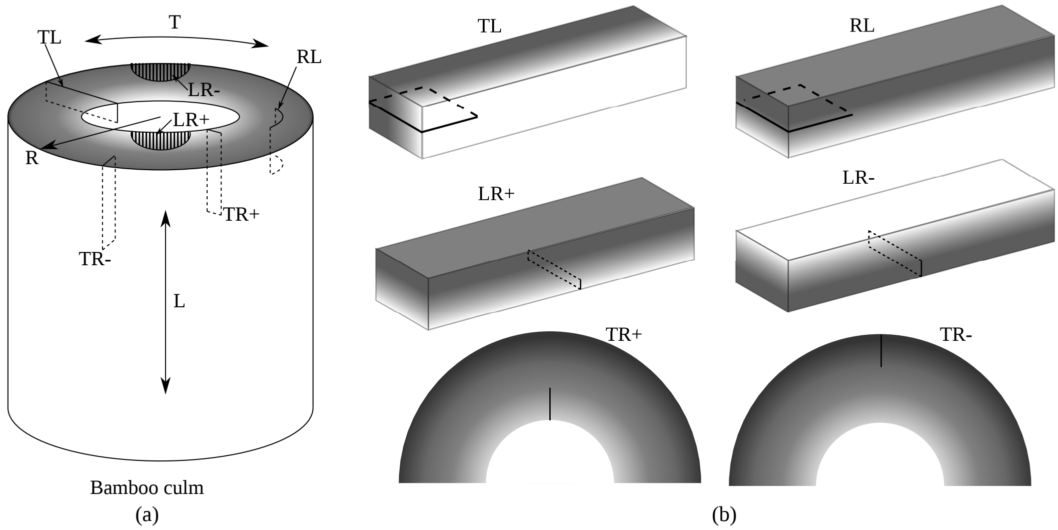

Figure 2: The six modes of crack propagation identified in bamboo. (a) A bamboo internode showing possible cracks that corresponds to the configurations tested. Each configuration in (a) is elaborated and drawn separately in (b).

image correlation (DIC) on two different specimens is reported to characterise the radial variations in axial and transverse moduli over the cross section. The transversely isotropic, radially graded properties are utilised to perform FE simulations on a 10 m tall bamboo subjected to tractions due to wind loads. These simulations, described in Sec. 3 elucidate the stress profiles and root moments that the bamboo experiences while it undergoes large scale bending. The characterisations of toughnesses in the various modes shown in Fig. 2 are described in Sec. 4. Pointers to a possible reason for the functional grading in bamboo are provided in Sec. 5. The salient conclusions from this work are enumerated in Sec. 6.

2. Stiffness of bulk bamboo

A bamboo culm of local variety (species *Dendrocalamus strictus*) was obtained from the botanical nursery, IIT Kanpur, India and aged in the open for eight weeks for natural seasoning. The sixth internode from bottom end of the culm (outer diameter 71.8, inner diameter 32.4 and length 270 mm) was selected for all experimental studies reported in this paper.

As mentioned earlier, two different samples, shown in Fig. 3(a) and (b), were used to heuristically characterise the complete stiffness matrix of bulk bamboo. The first sample is used to conduct DIC measurements on the RL plane while the semi-circular sample in Fig. 3(b) is used for measurements on the RT plane. The first sample was loaded in a four point bend setup while the section shown shaded was imaged. Similarly, the sample in Fig. 3(b) was loaded in tension and the region that was imaged is again shown shaded. In both cases, the displacement fields are expected to be symmetric about the y axis.

The displacement fields obtained from DIC (images were taken with a Grasshopper 3, MONO USB3 5.0 megapixel camera at 15 fps and analysed with the commercial DIC software Vic-2D from Correlated Solutions, USA) have a latent rigid body translation and rotation and suffer from slight lack of symmetry about the y axis. Small misalignments in the applied loads are known to cause these deviations.

In case of both specimens, displacement fields in the $x > 0$ region were corrected for rigid body rotation and lack of symmetry about $x = 0$. The displacement field at the i-th data point (x_i, y_i) (total number of data points is denoted by $2N$, i.e. N each from the domains $x > 0$ and $x < 0$) is denoted by $(u^{\mathrm{DIC}}(x_i, y_i), v^{\mathrm{DIC}}(x_i, y_i))$. The displacement field at the same data point, after correcting for rigid

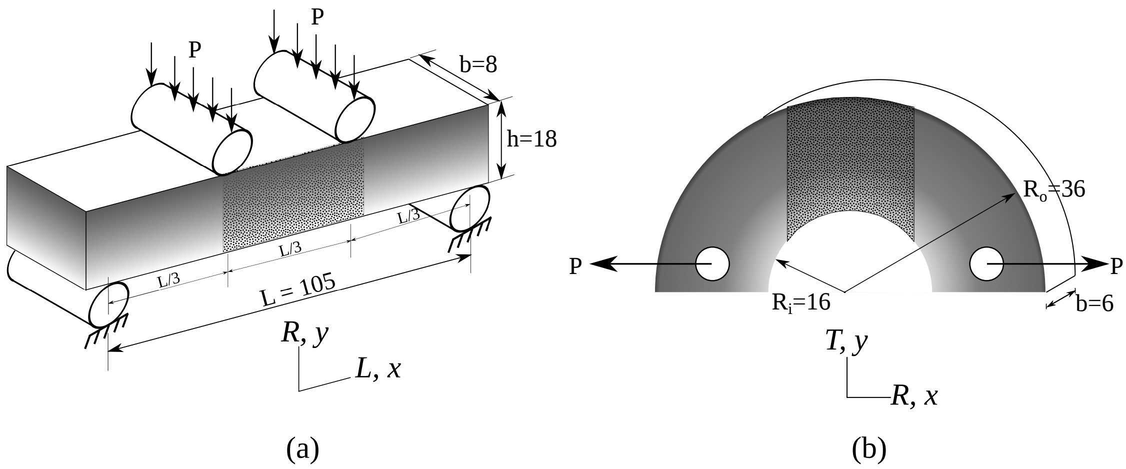

Figure 3: Specimens used to conduct DIC experiments on bamboo. (a) A specimen extracted from RL plane under four point bending. A semi-circular specimen from RT plane under tension is shown in (b). The dark shaded regions indicate the domains for DIC measurements.

body rotation, translation and lack of symmetry is denoted by $(u^{\text{corr}}(x_i, y_i), v^{\text{corr}}(x_i, y_i))$. The two sets of displacements are related through the following relations:

$$\begin{aligned} u^{\text{DIC}}(x_i, y_i) &= u^{\text{corr}}(x_i, y_i) + \alpha + x_i + y_i\theta \text{ and} \\ v^{\text{DIC}}(x_i, y_i) &= v^{\text{corr}}(x_i, y_i) + \beta - x_i\theta + y_i, \end{aligned} \tag{1}$$

subject to the symmetry condition about $x = 0$:

$$\begin{aligned} u^{\text{corr}}(-x_i, y_i) &= -u^{\text{corr}}(x_i, y_i) \text{ and} \\ v^{\text{corr}}(-x_i, y_i) &= v^{\text{corr}}(x_i, y_i). \end{aligned} \tag{2}$$

In the above $(\alpha,\ \beta)$ denote the rigid body translation, while θ denotes the angular rotation (assumed small) latent in the DIC measurements. A least squares problem is then set up by demanding that the total squared error

$$\Pi = \sum_{i=1}^{N} \left\{ \left[u^{\text{DIC}}(-x_i, y_i) - u^{\text{corr}}(-x_i, y_i)\right]^2 + \left[v^{\text{DIC}}(-x_i, y_i) - v^{\text{corr}}(-x_i, y_i)\right]^2 \right\}, \tag{3}$$

between the measured and corrected displacements on the $x < 0$ part of the imaged domain, is minimised. Further, using the fact that the corrected displacements on $x < 0$ should be related to those on the $x > 0$ part through eq. 2, the total squared error is rewritten as:

$$\begin{aligned} \Pi = \sum_{i=1}^{N} \Big\{ &\left[u^{\text{DIC}}(-x_i, y_i) + u^{\text{DIC}}(x_i, y_i) - \alpha - x_i - y_i\theta\right]^2 + \\ &\left[v^{\text{DIC}}(-x_i, y_i) - v^{\text{DIC}}(x_i, y_i) + \beta - x_i\theta + y_i\right]^2 \Big\}. \end{aligned} \tag{4}$$

The parameters α, β and θ are obtained in a least squares sense by minimising Π. Here, two typical instances of applying the correction on the displacements have been shown. In Fig. 4(a), the corrected displacements in the x direction are plotted on the corresponding uncorrected one. Similarly, for the semi-circular specimen, the corrected and uncorrected x displacements are shown in Fig. 4(b).

The elastic stiffness $\mathbb{C}$ of a transversely isotropic material in a Cartesian system spanned by the

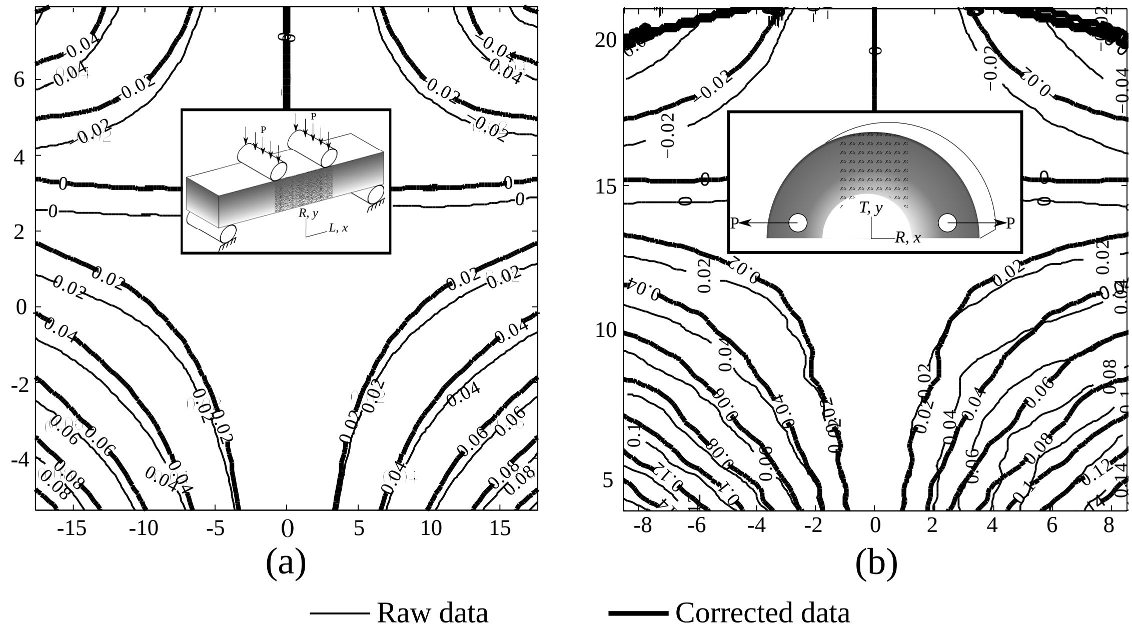

Figure 4: Comparison of x-displacement before and after applying the correction on the displacements in (a) four point bend and (b) semi-circular tension specimens. The loading configurations are shown in inset.

bases $\boldsymbol{e}_i$ (where, $\boldsymbol{e}_2, \boldsymbol{e}_3$ span the plane of isotropy) can be written as:

$$\mathbb{C} = \begin{pmatrix} C_{11} & C_{12} & C_{12} & 0 & 0 & 0 \\ \cdot & C_{22} & C_{23} & 0 & 0 & 0 \\ \cdot & \cdot & C_{22} & 0 & 0 & 0 \\ \cdot & \cdot & \cdot & C_{44} & 0 & 0 \\ \cdot & \cdot & \cdot & \cdot & (C_{22} - C_{23})/2 & 0 \\ \cdot & \cdot & \cdot & \cdot & \cdot & C_{44} \end{pmatrix}. \tag{5}$$

The stiffnesses C_{ij} can also be expressed in terms of the axial Young's modulus E^A, transverse Young's modulus E^T, shear moduli G^A, G^T and Poisson's ratios ν^A, ν^T through standard relations.

An attempt is now made to fit functions of the form $A\exp(kr)$, where A and k are constants to be determined, to each of the moduli, E^A, E^T, G^A and G^T. The choice of the function for describing the gradation in the moduli stems from the results in an earlier paper (Mannan et al., 2016), which is reviewed here briefly for the sake of continuity.

In Mannan et al. (2016), it has been shown that starting from the stiffness and orientation of the reinforcing microfibrils, it is possible to estimate the longitudinal stiffness of a fibre and ultimately a fibre bundle. The sequence of calculations is depicted in Fig. 5. The stiffness of a cellulose monoclinic I_β unit cell (see, Fig. 5(a)) is determined from molecular mechanics calculations. Including the amorphous hemicellulose-lignin, which forms 47 % of the basic building block and surrounds the mainly single-crystalline cellulose, the composite stiffness of the single fibre in the $\boldsymbol{a}_\alpha$ coordinate system can be obtained (see, Fig. 5(b)). Further, experimental measurements (see, Mannan et al., 2017) suggest that the average orientation of the microfibrils in fibres, i.e. $\bar{\mu}$, is 15°, with values ranging between $4 - 29°$. Synthetic fibre bundles can now be constructed (see, Fig. 5(c)) where the distribution of inner and outer diameters of the individual fibrils and the microfibril angles were assigned randomly from the experimentally determined actual distributions. The effective moduli computed from these synthetic fibre bundles were compared against nanoindentation studies and uniaxial tests on isolated

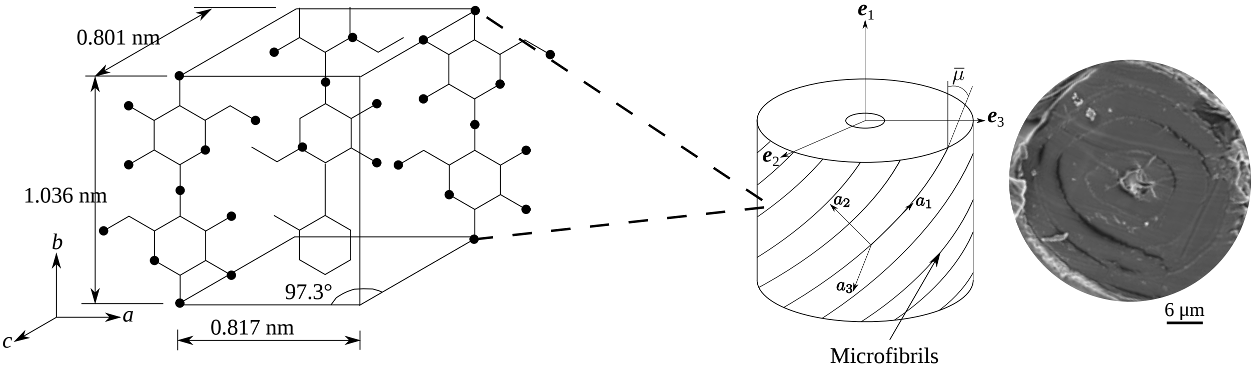

Cellulose microfibril	E^A	E^T	G^A	G^T	ν^A	ν^T
	137.6	15.7	4.2	5.4	0.09	0.46

Hemicellulose-lignin complex	E	ν
	7.8	0.5

(a)

Fibre	E^A	E^T	G^A	G^T	ν^A	ν^T
	74.4	5.9	2.3	1.9	0.19	0.43

(b)

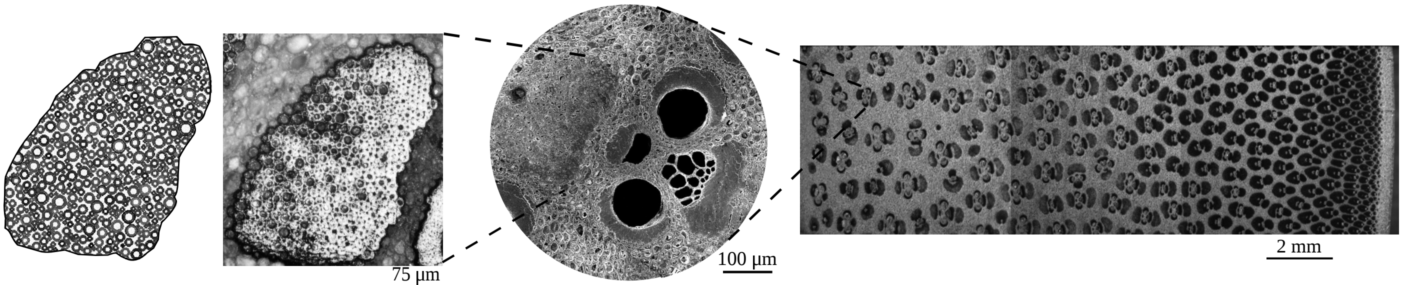

Fibre bundle	E^A	E^T	G^A	G^T	ν^A	ν^T
	20.1	2.6	0.98	0.84	0.18	0.51

(c)

Parenchyma matrix	E	ν
	4.45	0.34

(d)

Bamboo	E^A	E^T	G^A	G^T	ν^A	ν^T
	Refer column 5 of Table 1.					

(e)

Figure 5: Values of stiffnesses (in GPa) and Poisson's ratios of (a) cellulose monoclinic I_β crystal, (b) a single fibre in the $\boldsymbol{a}_\alpha$ coordinate system, (c) a fibre bundle, (d) parenchyma matrix idealised as a closed-cell foam and (e) bulk bamboo.

fibre bundles.

Similarly, in the parenchyma cell walls, cellulose content is low (about 33 %) while the MFA is much larger ($\simeq 33°$). The same procedure outlined for the fibre bundles also yields the stiffness properties of the parenchyma cell walls. The parenchyma matrix is considered to be isotropic closed-cell foam. With the cell wall properties and geometric parameters of the large parenchyma cells (see Mannan et al., 2016), relations in Gibson and Ashby (1997) allow us to derive the isotropic moduli and Poisson's ratio for the closed-cell foam structure (see, Fig. 5(d)). Now, with the stiffness matrix for the transversely isotropic fibre bundles and isotropic parenchyma matrix determined, a simple 'rule of mixtures' approach allows the determination of the overall transversely isotropic stiffness (see, Fig. 5(e)). This stiffness follows the variation of the areal density v_f of the much stiffer fibre bundles.

This exercise yields the variation of the moduli E^A, E^T, G^A, G^T; they seem to be well represented by the exponential variation of the form $A\exp(kr)$. The values of these moduli obtained for the fibre bundles and parenchyma cell walls are given in Table 1. The rule of mixtures based estimates for the radially graded moduli for the overall bamboo are also listed in the fifth column of this table. These estimates form the initial guess using which, the moduli and Poisson's ratios are determined heuristically, appropriate for the tested bamboo specimens.

The parameters of the radial variations were then fitted to match the corrected displacement fields obtained from DIC at a number of load levels. A close match of the u and v displacements in both the RL and RT planes were ensured at all these load levels. The FEM simulations were conducted using ABAQUS/Standard (ABAQUS, 2011). A user material subroutine (UMAT) was used where

	Parenchyma		Fibre bundle	Bamboo (predictions)	Bamboo (from DIC)
Young's modulus (GPa)	4.45 ± 2.62	Axial	20.1 ± 0.15	$0.99\exp(0.09r)$	$1.23\exp(0.08r)$
		Transverse	2.64 ± 0.01	$0.87\exp(0.003r)$	$0.56\exp(0.016r)$
Shear modulus (GPa)	1.67 ± 0.98	Axial	0.84 ± 0.01	$0.35\exp(0.02r)$	$0.5\exp(0.05r)$
		Transverse	0.98 ± 0.01	$0.38\exp(0.02r)$	$0.46\exp(0.03r)$
Poisson's ratio	0.34	Axial	0.18	0.34	0.36
		Transverse	0.51	0.36	0.19

Table 1: Values of stiffnesses and Poisson's ratios of the parenchyma matrix idealised as a closed cell foam, fibre bundles and bulk bamboo. The data in the second, fourth and fifth columns are obtained by the method outlined in Mannan et al. (2016). Note that the properties of bulk bamboo are graded with r in mm. The predicted values for bamboo follow from using the rule of mixtures on the predicted values of stiffnesses of the fibre bundles and parenchyma matrix. The more accurate estimates obtained from DIC, are given in the last column.

the radially graded transverse isotropy following the functional form $A\exp(kr)$ was incorporated. The aim was to determine the values of A and k for each of the moduli E^A, E^T, G^A, G^T such that the displacements from FEM match those from DIC. For the $x < 0$ parts of the domains, the comparisons between the FEM and DIC displacements at load levels corresponding to load point displacements of 2 mm, are shown in Fig. 6. These comparisons are obtained when the moduli chosen were those given in the last column of Table 1. Subsequent simulations are conducted with these moduli and Poisson's ratios.

3. Bamboo subjected to wind loads

With the radially graded transversely isotropic properties determined in the last section, the performance of a vertical bamboo cantilever subjected to wind loads will now be looked at. It should however, be noted that, the properties have been determined for a particular internode. Elastic properties also vary with position of the internode, with the younger ones near the tip being less stiff than the ones below. The radial variation of the moduli of the form $\sim A\exp(kr)$ has been taken all along the length of the bamboo. The structural models for bamboo, simulated in ABAQUS/Standard (ABAQUS, 2011) using 8-node linear brick elements (C3D8 in ABAQUS notation) and the UMAT described in the previous section are shown in Fig. 7(a). Large deformations and rotations were allowed. Three different cases have been analysed:

(i) A 10 m tall bamboo with a uniform annular cross section with all moduli equal to the average over the thickness, i.e. the homogeneous moduli are $\sim (1/(r_0 - r_i)\int_{r_i}^{r_0} A\exp(kr)\mathrm{d}r$, where the inner and outer radii are r_i and r_0, respectively. This will be referred to as the 'straight homogeneous' case.

(ii) An equally tall bamboo with homogeneous moduli, with same inner and outer radii as the straight homogeneous case at the root, i.e. $X_3 = 0$ but tapering towards the top. This is the 'tapered homogeneous' case.

(iii) A tapered bamboo with properties varying in the radial direction, a 'tapered graded' case.

All the three structures are subjected to the same wind load along the X_1 axis with a variation in the X_3 direction given by (Manwell et al., 2010):

$$\boldsymbol{v}(X_3) = v_0 \left(\frac{X_3}{X_0}\right)^{1/14} \boldsymbol{e}_1. \tag{6}$$

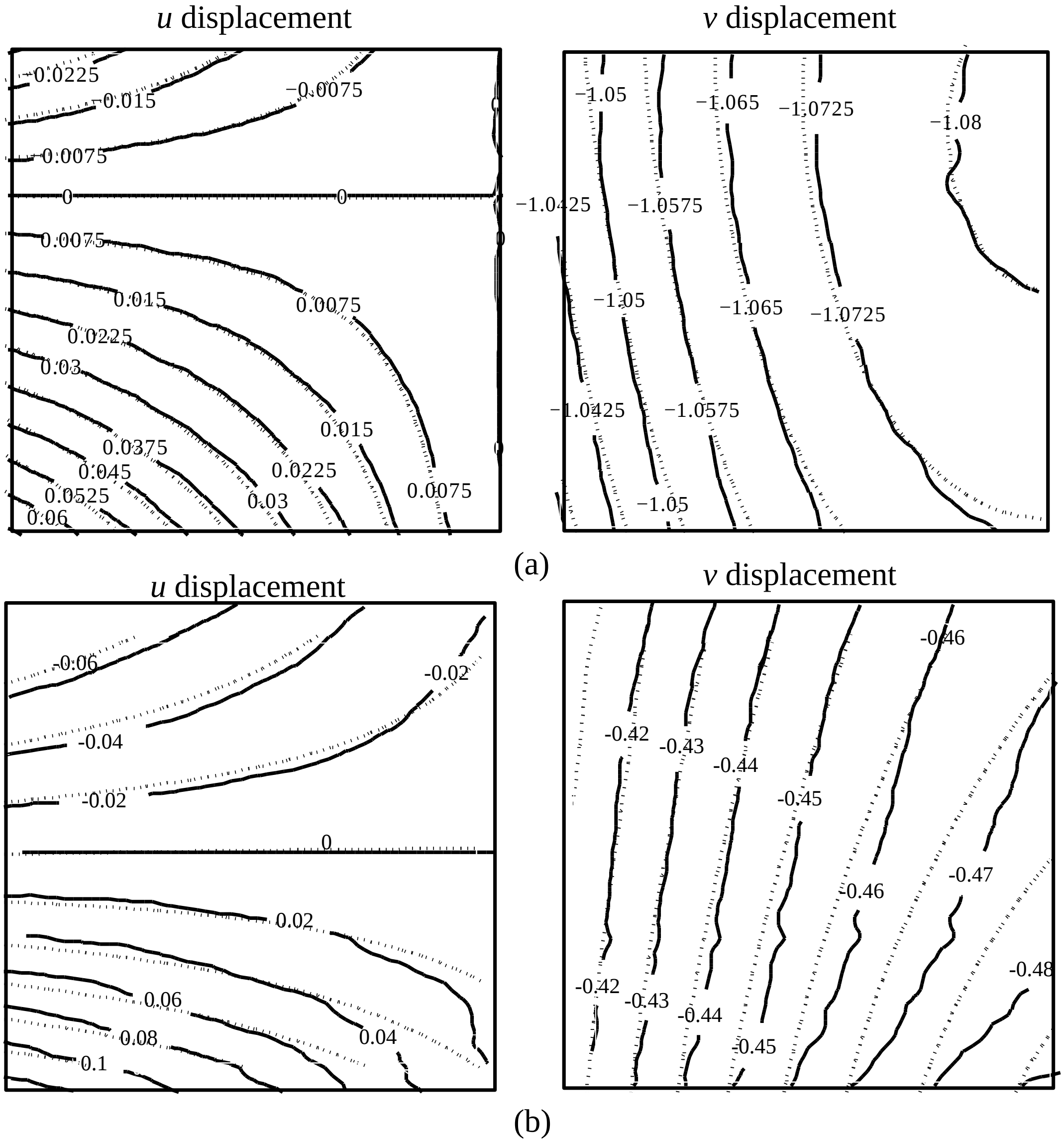

Figure 6: Comparisons between the FEM and DIC displacement fields corresponding to a load point displacement of 2 mm in (a) RL plane at 2178 N and in (b) RT plane at 138 N. Displacement field obtained through FEM analysis is plotted by dotted lines.

The normal traction on a surface with current outward normal $\boldsymbol{n}$ is computed as $\boldsymbol{t} = (1/2)C_{\mathrm{d}}\rho_{\mathrm{air}}|\boldsymbol{v}\cdot\boldsymbol{n}|^2$, where C_{d} is the drag coefficient. Note that, as the bamboo bends under the action of the wind load, $\boldsymbol{n}$ also keeps changing direction. While it is not intended to simulate particular loading conditions, realistic parameters (Manwell et al., 2010) were chosen for X_0, ρ_{air}, C_{d} and v_0 as 10 m, 1.2 kg/m^3, 1 and 16 m/s, respectively.

The deformed shapes of the bamboo under the applied wind load in the three cases are shown in Fig. 7(b). The reason for bamboo being tapered towards the top is clear from these results. The tip deflections (i.e. the position of the tip at $X_3/L = 1$) for the tapered cases are much larger than the homogeneous case. By deflecting more, the tapered bamboo reduces the wind load at the top and thereby, the moment at the root. The variation of the moment along the length is also shown in Fig. 7(c). For the straight homogeneous case, the moment at the root is much larger than the other cases. A straight, stiffer tall structure is much more likely to be uprooted by wind loads.

This mechanism has been shown to be operated in many other tall plants and water plants like the sea anemone *Metridium* (see, pp 376, Vogel, 2003). However, the axial stresses are the highest for $0 < X_3/L < 0.4$ and so, when a tapered structure breaks, it is likely to do so in this region.

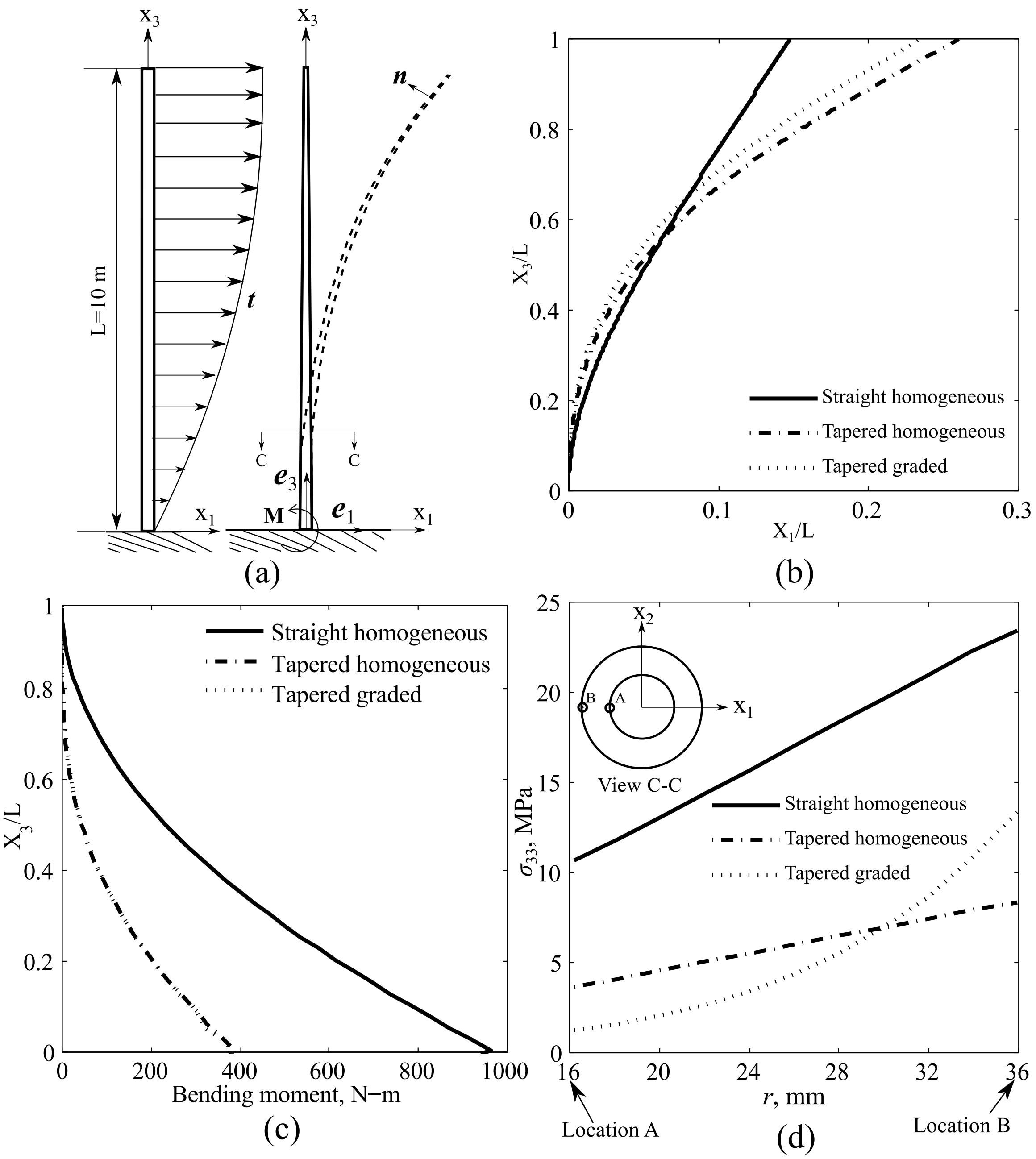

Figure 7: (a) The structural models for bamboo with typical traction distribution due to wind load. Variations of deflection and root moment with height are shown in (b) and (c), respectively. Distribution of longitudinal stress (σ_{33}) over the thickness at $X_3 = 0$ is plotted in (d).

The taper in bamboo arises because growth happens at the top. The culms towards the top are younger than those close to the root and hence have smaller diameters. The taper that this causes reduces the root moment. It is possible that by changing the taper profile with height, an even higher reduction in root moment could have been achieved. In other words, whether the taper profile in bamboo is structurally optimal is still an open question (see Sivanagendra and Ananthasuresh, 2009 for a similar discussion on wheat stalks).

The distribution of longitudinal stress over the thickness is shown in Fig. 7(d). The figure is for a cross-section at $X_3 = 0$, though similar variations are seen at any other cross-section. Clearly, if the bamboo is not tapered, σ_{33} at the root will be much higher. Taper reduces the stress levels considerably.

The advantages of the graded moduli are still not very clear. The levels of longitudinal stress across a cross section are not very different in the homogeneous and graded cases. The grading in moduli increases the longitudinal stress at the point B, compared to the homogeneous case. On the other hand,

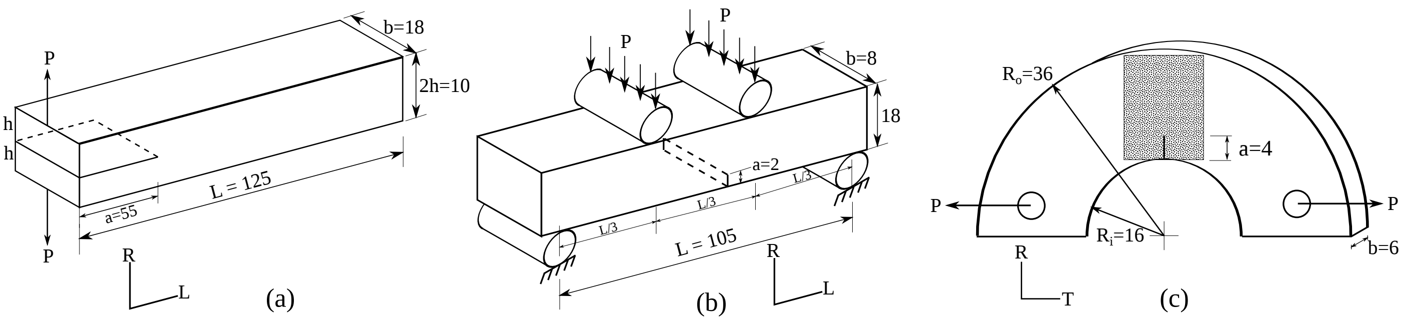

Figure 8: Specimens with dimensions and boundary conditions extracted from bamboo for calculating energy release rate. (a) Double cantilever beam specimens for G_{RL} and G_{TL}, (b) end-notched beam specimens for $G_{\mathrm{LR}\pm}$ and (c) arc-shaped tension specimen for $G_{\mathrm{TR}\pm}$.

the grading reduces the stress levels at the inner surface A. To understand why bamboo has evolved radially graded moduli (by varying the areal density of fibre bundles from 22 % at A to 62 % at B), it is worthwhile to study how the grading affects its tolerance to flaws.

4. Toughness of bamboo

Samples used to measure the toughness of a bamboo culm are shown in Fig. 2. As mentioned earlier, each configuration is identified by two letters denoting the direction normal to the crack plane and that of crack propagation, respectively. In the specimens used for measuring toughness in RL, TL, and LR± configurations, the fibre bundles are aligned along the length of the specimen. The variation in the areal fraction of fibres is indicated by the gradation in colour. In the TR± configurations, the fibres run into the plane. Moreover, the RL and TL modes are called as 'splitting modes', because the crack propagates by splitting the layers of fibres. On the other hand, LR± modes are 'cutting modes' where, the crack has to move ahead by cutting through the fibre bundles. In Fig. 2(a) possible cracks that will correspond to the configurations tested have been shown on a full culm.

Double cantilever beam (DCB) specimens have been used for testing the RL and TL configurations. The DCB specimens were fitted with piano hinges and procedures laid down in ASTM D5528 (ASTM D5528, 2013) were followed. In particular, load displacement traces, where the load was applied on the hinges through a universal testing machine (UTM) of 25 kN capacity, were used to calculate the energy release rate G through straightforward relations given in the standards.

In order to determine whether the fracture toughness is also radially graded, three sets of RL specimens have been used with a crack placed on the rarer side ($v_f = 0.22$), right in the middle ($v_f = 0.4$) and on the denser side ($v_f = 0.62$). The dimensions of the DCB specimens used are shown in Fig. 8(a). Figure 9(a) shows the variation of the energy release rate G_{RL} with crack extension Δa. Clearly, the energy release rate decreases with increased density of fibre bundles. In fact, as shown in Fig. 9(b), when normalised by the matrix volume fraction $(1 - v_f)$, the values of G_{RL} cluster around a value of around 2 kJ/m^2. This shows that the toughness of the softer matrix governs the splitting mode crack propagation in this configuration. Note that the axial stiffness E^A, has a trend that is opposite to G_{RL} and increases rapidly with v_f. Also, toughness of 0.5 to 2.0 kJ/m^2 in the splitting mode is higher than that of most varieties of wood and comparable to bone and many polymers.

Crack propagation in the TL configuration also proceeds in the splitting mode. The DCB specimen (see, Fig. 8(a)) has been used in this case as well. The variation of G_{TL} with Δa is shown in Fig. 10. In this case, the volume fraction of fibre bundles v_f varies along the crack front. The toughness G_{TL}

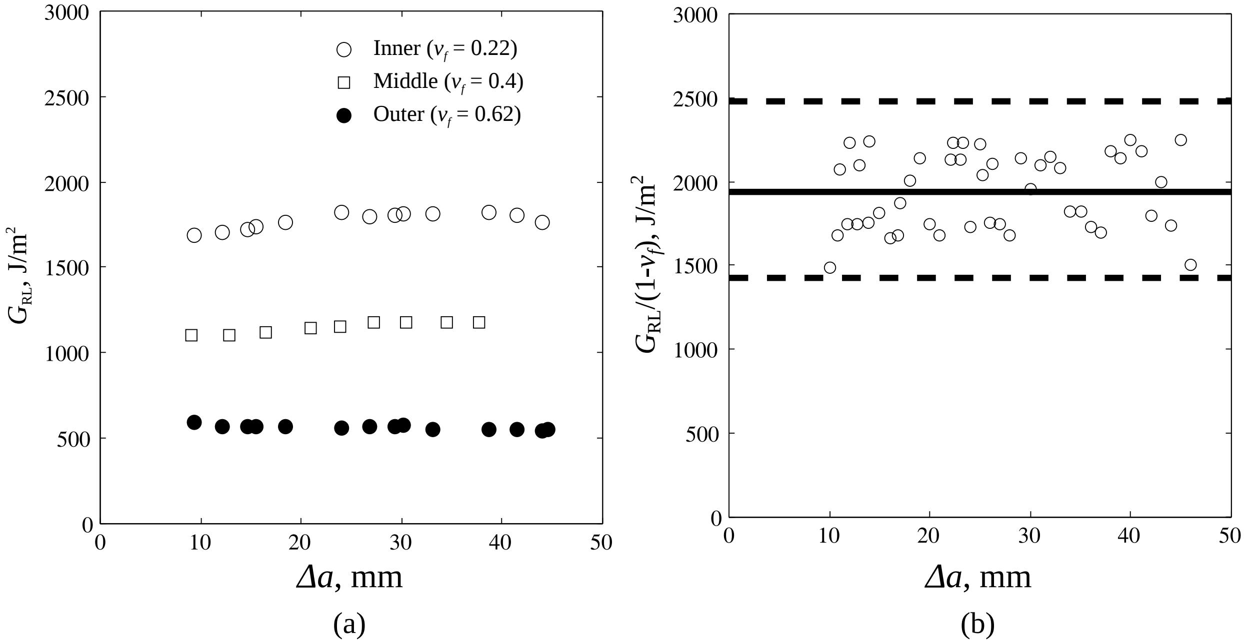

Figure 9: Energy release rate G in splitting modes in bamboo. (a) Variation of G_{RL} with crack extension Δa. (b) Normalised energy release rate $G_{\mathrm{RL}}/(1-v_f)$.

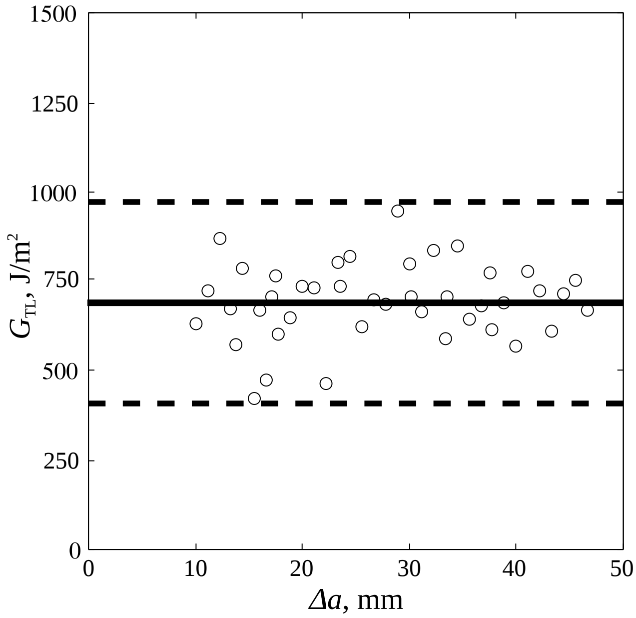

Figure 10: Energy release rate G_{TL} with each advance Δa measured using a DCB specimen. Here Δa is the average of crack advances noted on rear and far ends.

decreases from the rarer to the denser side. As a result, the crack front does not remain straight when the crack propagates (as also observed by Shao et al., 2009). The values of Δa in Fig. 10 are averages of the values noted from the near and far ends of the specimen. The toughness of ~ 0.75 kJ/m^2 is roughly the mean of the toughnesses at middle and outer region in Fig. 9(a).

Four point end-notched bend (ENB) specimens have been used to determine $G_{\mathrm{LR}\pm}(\Delta a)$. The dimensions of the specimen used are shown in Fig. 8(b). Anticipating that the toughnesses for the LR+ and LR− cases will be significantly different, to start with, rather short cracks have been used. This ensures that the v_f ahead of the LR+ crack is very different from the LR− one. The fracture toughness is experimentally computed by determining the compliance of the ENB specimen $C(a+\Delta a)$ whereby

$$G_{\mathrm{LR}\pm} = \frac{P^2}{2b}\frac{\mathrm{d}C}{\mathrm{d}\Delta a}. \tag{7}$$

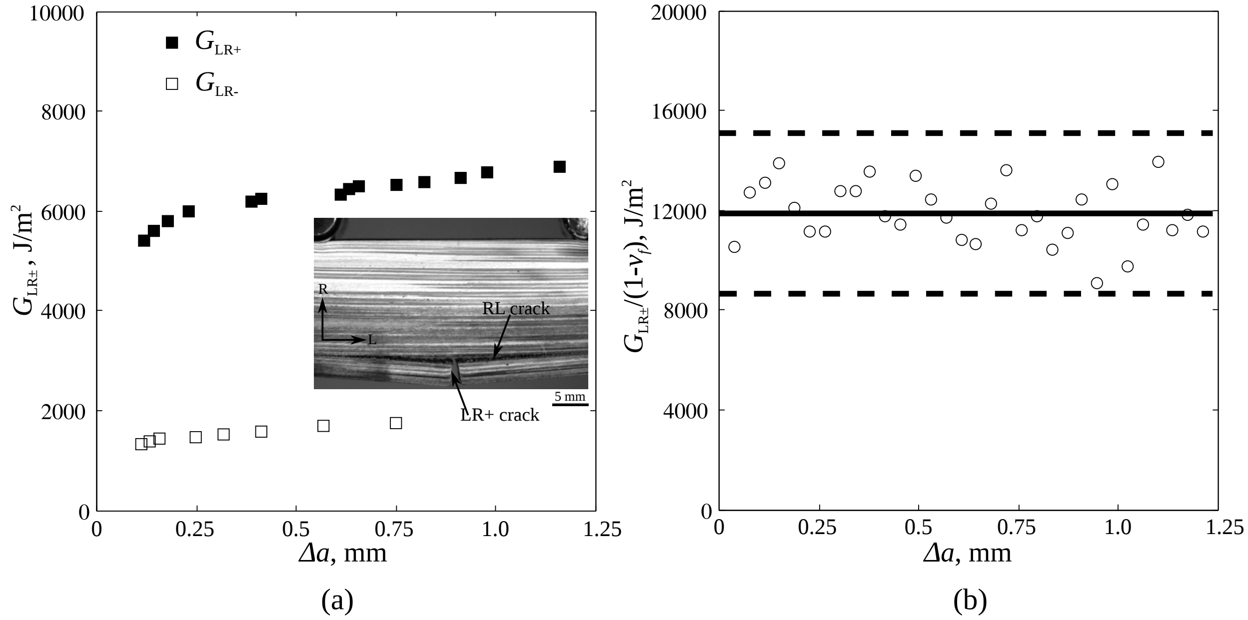

Figure 11: Energy release rates G in fibre-cutting modes in bamboo. (a) Variation of $G_{\mathrm{LR}\pm}$ with crack extension Δa. (b) Normalised energy release rate $G_{\mathrm{LR}\pm}/(1 - v_f)$.

The results are shown in Figs. 11(a) and (b). The resistance to a crack propagating from the rarer side (i.e. LR+ configuration) is 3.5 times that of a crack propagating from the denser side. But, again, when scaled by the matrix volume fraction, $(1 - v_f)$ at the tip of the crack, the toughnesses of both the configurations (see, Fig. 11(b)) collapse to around 12 kJ/m^2. This indicates that in the LR$\pm$ configurations, the crack grows by avoiding the fibre bundles and most of the resistance to crack growth is from the matrix. Also note that, bamboo is much more resistant to fracture in the cutting mode than in the splitting modes. In fact, in the experiments, a crack in the LR$\pm$ configuration grows very little (eg. an initially 2 mm crack grows by about 0.75 mm in the LR- mode and 1.1 mm in the LR+ mode before kinking) in the R direction and readily gives rise to a RL crack in the splitting mode, as shown in the inset of Fig. 11(a). The toughness $G_{\mathrm{LR}\pm}$ is basically the value at initiation.

The toughnesses in the TR$\pm$ configurations are more difficult to determine. The annular samples used for this purpose are shown in Fig. 8(c). Here, DIC is used to map the displacement field in the area close to the crack tip (shown shaded in Fig. 8(c)). These displacement fields are compared with the asymptotic near tip displacement fields for an anisotropic elastic material given by eq. 20 in Sih et al. (1965). The undetermined parameter in these equations is K_{I}, the mode-I stress intensity factor, which is fitted by comparison with the DIC fields. The toughness $G_{\mathrm{TR}\pm}$ is then obtained using its relation with K_{I} (given again by eq. 26 of Sih et al., 1965). As shown in Fig. 12, the values of $G_{\mathrm{TR}\pm}$ are very close (2.1 kJ/m^2 for a crack starting from the rarer end compared to 2.6 kJ/m^2 for one starting from the denser end), indicating that TR$\pm$ cracks will propagate with equal ease in the radial direction, irrespective of whether they are located at the rarer or denser end. Note that the TR plane is the plane of isotropy.

The TR crack, in a bamboo culm represents a splitting crack along the longitudinal direction. In bending under wind loads, a TR$\pm$ crack does not pose much danger of failure as the hoop stress generated in the bamboo due to bending is much smaller than σ_{33}.

It is worthwhile at this stage to review the fracture toughness data obtained for the various configurations. Note from Fig. 7(d) that the axial stress in a bamboo under bending due to wind load is lowest at the rarer end and highest at the outer, denser end. In fact, if the bamboo cross section was

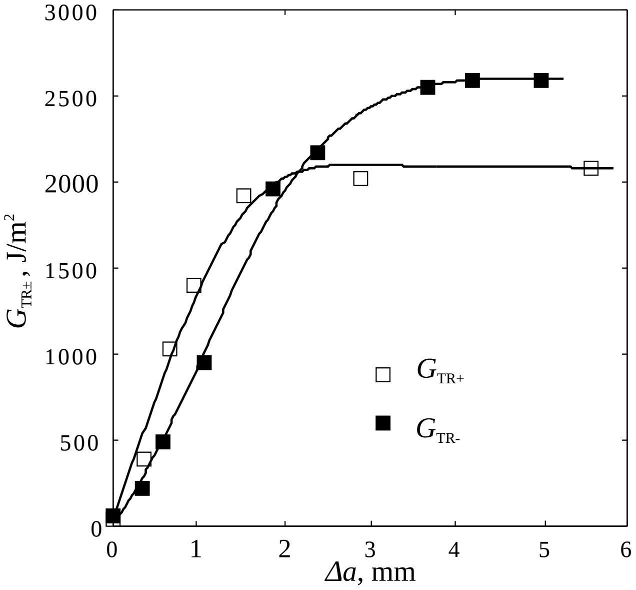

Figure 12: Energy release rates $G_{\mathrm{TR}\pm}$ with each advance Δa measured using an arc tensile specimen shown in Fig. 8(c).

not radially graded and had a uniform axial modulus equal to the average value, the axial stress at the outer end (point B, in Fig. 7(d)) would have been significantly lower. Gradation acts to elevate the stresses at B, which is also the point in any cross section with the maximum axial tensile stress.

The toughnesses in the splitting RL and cutting LR$\pm$ configurations are high at the rarer end and low at the outer, denser end. In light of the discussion above, this seems paradoxical. The toughness seems to be low at a region where the stresses due to bending are actually elevated by virtue of the gradation in moduli. In the next section, a possible solution to this paradox is provided.

5. Why does bamboo have radially graded properties?

Consider a LR$-$ flaw on the outer surface of the bamboo culm as shown in Fig. 13. Further assume that the culm is located at a location where the bending stress σ_{33} is high. The magnitude of the stress experienced varies with the wind speed but the nature of the variation across the thickness is as shown in Fig. 7(d). In the LR$-$ configuration, the crack is subjected to a remote load given by the distribution of σ_{33}, as shown in Fig. 7(d).

An attempt is now made to find out when, given a wind speed v_0, a LR$\pm$ crack will kink into a RL crack in the manner shown in the inset of Fig. 11(a). Recall that the toughness of a crack emanating from the inner side, i.e. in the LR+ configuration, is a few times higher than for one from the outer side. Similarly, the toughness of a splitting crack (i.e. in the RL configuration), is much lower than the crack in the cutting mode and is higher when the crack is located close to the inner surface. Thus, the transition of a LR$\pm$ crack into a RL crack is likely to be governed by the relative magnitudes of the toughnesses in the cutting and splitting modes.

Consider the stress field ahead of a small 90° kink of length ζ from a main LR$-$ crack of length a, as shown in Fig. 13. The main crack is subjected to remote loads $\sigma_{33}(x_1)$. The modes I and II stress intensity factors k_1 and k_2 at the tip of the kink are given by

$$
\begin{aligned}
k_1(a) &= \lim_{r\to 0} \sqrt{2\pi\zeta} K_{\mathrm{LR}-}(a) f^1_{yy}\left(\mu_1(a), \mu_2(a), \frac{\pi}{2}\right)\\
k_2(a) &= \lim_{r\to 0} \sqrt{2\pi\zeta} K_{\mathrm{LR}-}(a) f^2_{xy}\left(\mu_1(a), \mu_2(a), \frac{\pi}{2}\right),
\end{aligned}
$$

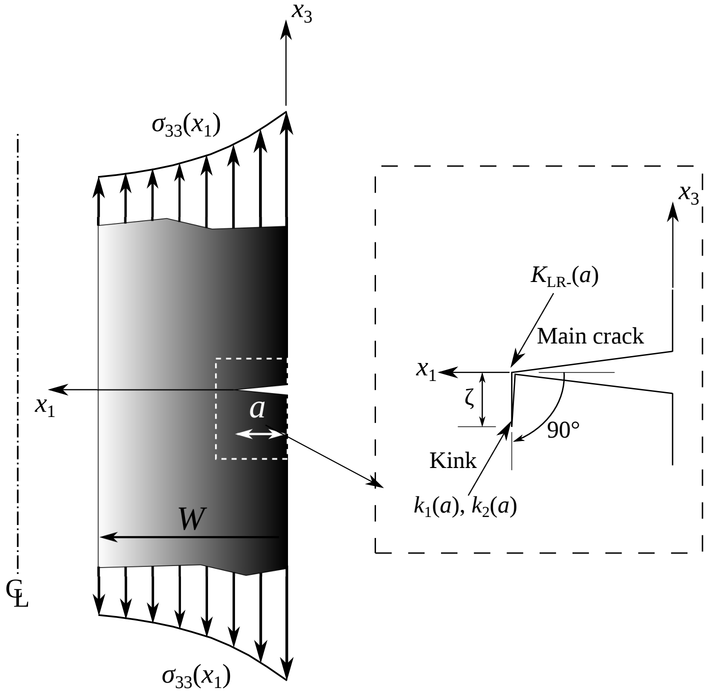

Figure 13: A crack of length a in the LR$-$ configuration subjected to a remote stress σ_{33} akin to the one shown in Fig. 7(d). The stress intensity factors $k_1(a)$ and $k_1(a)$ at the tip of incipient kink ($\zeta \to 0$) is determined in the text.

where $K_{\mathrm{LR}-}(a)$ is the mode I stress intensity factor to which the main LR$-$ crack is subjected due to the remote load $\sigma_{33}(x_1)$. Further, $\mu_{1,2}(x_1)$ are complex roots of a fourth order polynomial equation whose coefficients depend on the components of the compliance tensor $\boldsymbol{S} = \boldsymbol{C}^{-1}$ for the transversely isotropic material. The roots are functions of the length a of the main crack as the components of the compliance tensor vary with grading in x_1. Also, for the main crack (Bao et al., 1992)

$$K_{\mathrm{LR}-}(x_1) = \sigma_{33}(x_1)\sqrt{\pi a}\, Y(\eta(x_1))\; F(a/W), \tag{8}$$

where

$$\eta(x_1) = \frac{\sqrt{E^A(x_1)\; E^T(x_1)}}{2\; G^A(x_1)} - \nu^A \sqrt{\frac{E^T(x_1)}{E^A(x_1)}}. \tag{9}$$

The angular functions $f^1_{yy}(\mu_1, \mu_2, \theta)$ and $f^2_{xy}(\mu_1, \mu_2, \theta)$, the factor $Y(\eta)$ and the shape function $F(a/W)$ are reproduced in AppendixA, for the sake of completeness, from Sih et al. (1965) and Bao et al. (1992), respectively. Once $k_1(a)$ and $k_2(a)$ are obtained (in the case where the roots μ_1 and μ_2 are distinct) for a given LR$-$ crack of length a, the energy release rate for the kink can be derived easily from Sih et al. (1965),

$$\mathcal{G}_{\mathrm{RL}}(a) = -\frac{\pi k_1}{2} S_{22} \mathrm{Im}\left[\frac{k_1(\mu_1+\mu_2)+k_2}{\mu_1\mu_2}\right] + \frac{\pi k_2}{2} S_{11} \mathrm{Im}\left[k_2(\mu_1+\mu_2)+k_1\mu_1\mu_2\right]. \tag{10}$$

This is the crack driving force for the kink in Fig. 13. In other words, a fibre cutting LR$-$ crack will kink into a splitting RL crack when

$$\mathcal{G}_{\mathrm{RL}}(a) = G_{\mathrm{RL}}(a), \tag{11}$$

where G_{RL} is measured experimentally in the previous section. Also, as $G_{\mathrm{LR}-} >> G_{\mathrm{RL}}$ for all values of a, as wind velocity v_0 increases, the condition for propagation of the kink in the RL configuration eq. 11, will always be satisfied before the LR$-$ crack can propagate straight along x_1. The relative values of $G_{\mathrm{LR}\pm}$ and G_{RL} ensure that a crack in the LR$\pm$ configuration always kinks and grows as a RL one.

A crack in the LR$\pm$ configuration, if it can propagate through the thickness of the culm, will cause the entire structure to fail. However, allowing a LR$\pm$ crack to kink into a splitting mode RL crack will, at worst, cause a loss of the cross section (and therefore bending stiffness) but will not disrupt the entire structure. It is also possible that the RL crack will be arrested at the nodes. Note that a full grown bamboo has $50 - 100$ internodes and the structure may easily survive even if one of them is cracked. Therefore, if the LR$-$ crack kinks easily, the extent of loss in bending stiffness will be minimised.

The values of critical energy release rates at which LR$\pm$ cracks in a graded transversely isotropic material or a homogeneous isotropic material kink, can be determined in the same way. It is instructive to compare the remote stresses σ_{33} required to initiate kinking in cracks in all these cases, as a function of the normalised crack length a/W. The homogeneous case (with stiffness and fracture properties taken as averages of the graded values over the radius), is presented in Figs. 14(a) and (b) while those for the actual graded case are presented in Figs. 14(c) and (d). The stress distributions across the most stressed cross sections in each case are also plotted for different wind velocities.

For all Figs.14(a)-(d), the thick solid curves indicate, for various values of a/W, the stress σ_{33} at which a LR$\pm$ crack kinks into a RL crack. The distributions of the axial stress over the most stressed cross sections are shown with light solid lines for different wind velocities.

Consider now a short LR$\pm$ flaw of, say, $a/W = 0.2$. If bamboo cross sections were made up of a homogeneous material, this flaw, will kink when the wind speed is 18 and 23 m/s in the LR$-$ and LR$+$ configurations, respectively. For the homogeneous case, the LR$\pm$ configurations are completely symmetric except for the small difference caused by the variation of the remote bending stress.

In the graded case, as seen from Figs. 14(c) and (d), the internal LR$+$ crack of size $a/W = 0.2$ will withstand a much higher wind speed (about 41 m/s) than an external LR$-$ crack. If the flaw sizes are smaller, the difference in wind speeds at which kinking happens is even larger.

Thus LR$-$ cracks on the outside will kink at low wind velocities. On the other hand, LR$+$ cracks of the same length will withstand higher wind velocities before they kink.

6. Conclusions

Bamboo culms are transversely isotropic materials with the axial direction being the axis of symmetry. Moreover, all stiffnesses are graded in the radial direction owing to the much denser distribution of the fibre bundles at the outer periphery. The axial and transverse moduli have been characterised for one particular variety of bamboo. As all species of bamboo have gradation in fibre bundle density, it is expected that their characterisation as 'radially graded transversely isotropic' materials is valid in general.

Further, the fracture toughnesses of cracks oriented in different configurations have been calibrated. Two configurations seem especially important. In the RL configuration, the crack propagates rather easily in a splitting mode, while in the LR$\pm$ configurations, the fracture resistance is much higher because the crack, in order to advance, has to cut through the hard fibre bundles. In all cases, the toughnesses determined experimentally are higher at the inner radius than at the outer, exactly opposite of how the stiffnesses vary.

It has been also shown that under mode I loading common in bamboo structures subjected to wind loads, before a LR$\pm$ crack propagates, it will, in all likelihood, kink at right angles and propagate as a splitting mode RL crack. The kinking seems to be a strategy that has evolved in order to protect the bamboo structure against complete failure under wind loads. A LR$\pm$ crack kinked into a RL one,

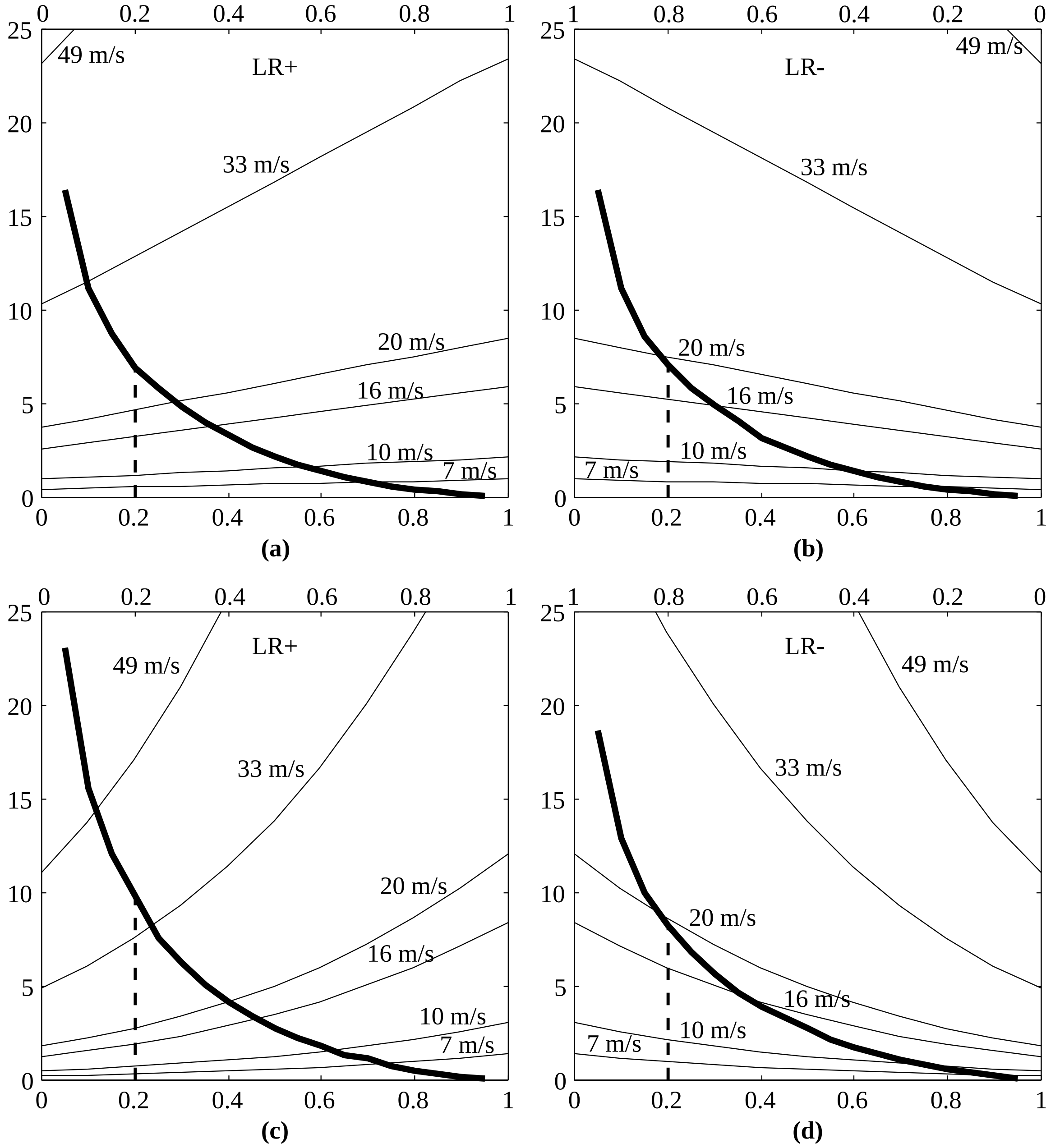

Figure 14: Comparisons of remote stresses σ_{33} required to initiate kinking in LR$\pm$ cracks. (a) LR+ crack in homogeneous isotropic material. (b) LR$-$ crack in homogeneous isotropic material. LR+ and LR$-$ cracks in the actual graded transversely isotropic material are shown in (c) and (d), respectively. On Y axis are plotted remote stress σ_{33} while lower and upper X axes represent a/W and $(r - r_i)/(r_o - r_i)$, respectively.

causes a loss of local flexural stiffness with the possibility that the resultant RL crack will be arrested by the nodes.

The typical gradation of moduli and fracture toughnesses over the radius in bamboo culms thus seems to achieve two purposes. The uprooting moment at the root of the structure is lower than it would have been if the bamboo was made up of a homogeneous material.

Moreover, when subjected to bending, even very small *external* flaws will kink easily, propagate as splitting cracks in the longitudinal direction and possibly get arrested at the nodes. This will limit the damage to a small loss in flexural stiffness but will not disrupt the entire structure. An internal flaw, on the other hand, will also kink, but at much higher wind loads. The distinctive distribution of toughnesses and stiffnesses over the radius observed in bamboo culms achieves the twin goal of reducing the damage causing potential of external flaws and at the same time, making the internal parts of the thickness resistant to bigger flaws.

Conflicts of interest

Conflicts of interest: none.

Funding statement

This research did not receive any specific grant from funding agencies in the public, commercial, or not-for-profit sectors.

AppendixA. Crack tip fields in anisotropic materials

The results from Sih et al. (1965) used for stress and displacement fields around the tip of a crack in an anisotropic material is summarised here for the sake of completeness. In a (r, θ) cylindrical polar coordinate system with origin at the tip of the sharp crack, the stresses are formulated in terms of the analytic functions, $\phi_j(z_j)$, of the complex variable, $z_j = x_j + iy_j$ (j=1, 2), where

$$x_j = x + \alpha_j y,\ y_j = y + \beta_j y\ (j = 1, 2). \tag{A.1}$$

The parameters α_j and β_j are the real and imaginary parts of μ_j i.e., $\mu_j = \alpha_j + i\beta_j$, as determined from

$$\mathbb{S}_{11}\,\mu^4 \;-\; 2\,\mathbb{S}_{14}\,\mu^3 \;+\; (2\,\mathbb{S}_{12} + \mathbb{S}_{44})\,\mu^2 \;-\; 2\,\mathbb{S}_{24}\,\mu \;+\; \mathbb{S}_{22} \;=\; 0, \tag{A.2}$$

where, $\mathbb{S}_{ij}$ are compliances. The roots μ_j of eq. A.2 are always complex or pure imaginary and will occur in conjugate pairs as $\mu_1,\ \bar{\mu}_1,\ \mu_2,$ and $\bar{\mu}_2$. The relations for the stresses σ_{xx}, σ_{yy} and σ_{xy} in a small region surrounding the crack in general anisotropic material for modes 1 and 2 are (Sih et al., 1965):

$$\begin{aligned}
\sigma_{xx} &= \frac{K_1}{\sqrt{2\pi r}} f^1_{xx}(\mu_1, \mu_2, \theta) = \frac{K_1}{\sqrt{2r}} \mathrm{Re}\Big[\frac{\mu_1\mu_2}{\mu_1 - \mu_2}\Big(\frac{\mu_2}{\sqrt{\cos\theta + \mu_2 \sin\theta}} - \frac{\mu_1}{\sqrt{\cos\theta + \mu_1 \sin\theta}}\Big)\Big] \\
\sigma_{yy} &= \frac{K_1}{\sqrt{2\pi r}} f^1_{yy}(\mu_1, \mu_2, \theta) = \frac{K_1}{\sqrt{2r}} \mathrm{Re}\Big[\frac{1}{\mu_1 - \mu_2}\Big(\frac{\mu_1}{\sqrt{\cos\theta + \mu_2 \sin\theta}} - \frac{\mu_2}{\sqrt{\cos\theta + \mu_1 \sin\theta}}\Big)\Big] \\
\sigma_{xy} &= \frac{K_1}{\sqrt{2\pi r}} f^1_{xy}(\mu_1, \mu_2, \theta) = \frac{K_1}{\sqrt{2r}} \mathrm{Re}\Big[\frac{\mu_1\mu_2}{\mu_1 - \mu_2}\Big(\frac{1}{\sqrt{\cos\theta + \mu_1 \sin\theta}} - \frac{1}{\sqrt{\cos\theta + \mu_2 \sin\theta}}\Big)\Big]
\end{aligned} \tag{A.3}$$

and

$$\begin{aligned}
\sigma_{xx} &= \frac{K_2}{\sqrt{2\pi r}} f^2_{xx} = (\mu_1, \mu_2, \theta) = \frac{K_2}{\sqrt{2r}} \mathrm{Re}\Big[\frac{1}{\mu_1 - \mu_2}\Big(\frac{\mu_2^2}{\sqrt{\cos\theta + \mu_2 \sin\theta}} - \frac{\mu_1^2}{\sqrt{\cos\theta + \mu_1 \sin\theta}}\Big)\Big] \\
\sigma_{yy} &= \frac{K_2}{\sqrt{2\pi r}} f^2_{yy}(\mu_1, \mu_2, \theta) = \frac{K_2}{\sqrt{2r}} \mathrm{Re}\Big[\frac{1}{\mu_1 - \mu_2}\Big(\frac{1}{\sqrt{\cos\theta + \mu_2 \sin\theta}} - \frac{1}{\sqrt{\cos\theta + \mu_1 \sin\theta}}\Big)\Big] \\
\sigma_{xy} &= \frac{K_2}{\sqrt{2\pi r}} f^2_{xy}(\mu_1, \mu_2, \theta) = \frac{K_2}{\sqrt{2r}} \mathrm{Re}\Big[\frac{1}{\mu_1 - \mu_2}\Big(\frac{\mu_1}{\sqrt{\cos\theta + \mu_1 \sin\theta}} - \frac{\mu_2}{\sqrt{\cos\theta + \mu_2 \sin\theta}}\Big)\Big].
\end{aligned} \tag{A.4}$$

In the analysis in Sec. 5, the calculations have been performed assuming a mode 1 crack in a finite sized end-notched bend specimen (shown in Fig. 8(b)), where, the stress intensity factor K_1 is given by (Bao et al., 1992):

$$
\begin{aligned}
K_1 &= \sigma\sqrt{\pi a}\,\mathrm{Y}(\eta)\,\mathrm{F}(a/W),\\
\eta &= \frac{\sqrt{E^A\,E^T}}{2\,G^A} - \nu^A\sqrt{\frac{E^T}{E^A}},\\
\mathrm{Y}(\eta) &= 1 + 0.1(\eta-1) - 0.016(\eta-1)^2 + 0.002(\eta-1)^3 \text{ and}\\
\mathrm{F}(a/W) &= \sqrt{\frac{2W}{\pi a}\tan\frac{\pi a}{2W}}\,\frac{0.752 + 2.02(a/W) + 0.37(1-\sin\frac{\pi a}{2W})^3}{\cos\frac{\pi a}{2W}}.
\end{aligned} \tag{A.5}
$$

References

ABAQUS, 2011. ABAQUS/Standard user's manual, Version 6.11. Dassault Systmes, Providence, RI, USA.

Amada, S., Untao, S., 2001. Fracture properties of bamboo. Composites Part B: Engineering 32 (5), 451–459.

ASTM D5528, 2013. Standard test method for mode I interlaminar fracture toughness of unidirectional fiber-reinforced polymer matrix composites.

Bao, G., Ho, S., Suo, Z., Fan, B., 1992. The role of material orthotropy in fracture specimens for composites. International Journal of Solids and Structures 29 (9), 1105–1116.

Gibson, L. J., Ashby, M. F., 1997. Cellular Solids: Structure and Properties. Cambridge Solid State Science Series. Cambridge University Press.

Liese, W., 1998. The anatomy of bamboo culms. Tech. Rep. 18, International Network for Bamboo and Rattan.

Mannan, S., Knox, J. P., Basu, S., 2017. Correlations between axial stiffness and microstructure of a species of bamboo. Royal Society Open Science 4 (1), 160412.

Mannan, S., Zaffar, M., Pradhan, A., Basu, S., 2016. Measurement of microfibril angles in bamboo using mueller matrix imaging. Applied Optics 55 (32), 8971–8978.

Manwell, J. F., McGowan, J. G., Rogers, A. L., 2010. Wind Energy Explained: Theory, Design and Application. Wiley.

Shao, Z. P., Fang, C. H., Tian, G. L., 2009. Mode I interlaminar fracture property of Moso bamboo (Phyllostachys Pubescens). Wood Science and Technology 43 (5-6), 527–536.

Sih, G. C., Paris, P. C., Irwin, G. R., 1965. On cracks in rectilinearly anisotropic bodies. International Journal of Fracture Mechanics 1 (3), 189–203.

Silva, E. C. N., Walters, M. C., Paulino, G. H., 2008. Modeling bamboo as a functionally graded material. In: AIP Conference Proceedings. pp. 754–759.

Sivanagendra, P., Ananthasuresh, G., 2009. Size optimization of a cantilever beam under deformation-dependent loads with application to wheat stalks. Structural and Multidisciplinary Optimization 39 (3), 327–336.

Tan, T., Rahbar, N., Allameh, S., Kwofie, S., Dissmore, D., Ghavami, K., Soboyejo, W., 2011. Mechanical properties of functionally graded hierarchical bamboo structures. Acta Biomaterialia 7 (10), 3796–3803.

Vogel, S., 2003. Comparative Biomechanics: Life's Physical World, Second Edition. Princeton University Press.

Wegst, U. G., 2011. Bending efficiency through property gradients in bamboo, palm, and wood-based composites. Journal of the Mechanical Behavior of Biomedical Materials 4 (5), 744 – 755.

Wegst, U. G. K., Ashby, M. F., 2004. The mechanical efficiency of natural materials. Philosophical Magazine 84 (21), 2167–2186.

Wegst, U. G. K., Bai, H., Saiz, E., Ritchie, R. O., 2014. Bioinspired structural materials. Nature Materials 14 (1), 23–36.

Zhao, J. T., Ma, S. P., Liu, H. R., Ren, H. Q., 1 2011. Experimental investigation of the mixed-mode crack expanding in bamboo. In: Advances in Superalloys. Vol. 146 of Advanced Materials Research. Trans Tech Publications, pp. 1285–1288.